Agricultural and Forest Meteorology 276–277 (2019) 107641

Contents lists available at ScienceDirect

Agricultural and Forest Meteorology

journal homepage: www.elsevier.com/locate/agrformet

Local land surface temperature change induced by afforestation based on satellite observations in Guangdong plantation forests in China

Wenjuan Shen[a,b], Mingshi Li[a,b,*], Chengquan Huang[c], Tao He[d], Xin Tao[e], Anshi Wei[f]

[a] College of Forestry, Nanjing Forestry University, Nanjing 210037, China
[b] Co-Innovation Center for Sustainable Forestry in Southern China, Nanjing Forestry University, Nanjing 210037, China
[c] Department of Geographical Sciences, University of Maryland, College Park, MD 20742, USA
[d] School of Remote Sensing and Information Engineering, Wuhan University, Hubei 430079, China
[e] Department of Geography, University at Buffalo, Buffalo, NY 14261, USA
[f] Guangdong Provincial Center for Forest Resources Monitoring, Guangzhou 510173, China

ARTICLE INFO

Keywords:
Plantation forests
Forest cover change
Temperature
ET
Albedo
Southern China

ABSTRACT

Estimating the effects of large scale afforestation is essential for the accurate understanding of its potential for the mitigation of climate warming. We used satellite observations to quantify the effects of the conversion of open lands (i.e., grassland and cropland) and natural forests to plantation forests and their associated biophysical processes (i.e., albedo and evapotranspiration (ET)) on land surface temperature (LST) in Guangdong Province, China. The hypothetical change (mean 2002–2018 values of LST difference between plantation forests and nearby lands in 2010) using the moving window searching-based method and actual change (changes of afforested area affecting the LST difference from 2000 to 2010) using the spatial pattern change trend method were detected in order to characterize the spatiotemporal variations in surface temperature, related albedo, and ET. The relationships between albedo, ET, and surface temperature change were also determined in combination with interpolated air temperature and precipitation. Results showed that the two methods-based afforestation changes had a similar net cooling effect, but a discrepancy in diurnal, seasonal, and spatial variations occurred. Overall, the actual change of afforested area led to a cooling effect by an average of -0.18 ± 0.02 °C, especially from croplands, which was greater than the air temperature. Individually, afforestation in the mid-subtropical forest zone (north of 24 °N, northern Guangdong) had a warming effect, especially during the transition from natural forests to plantation forests. We also observed an increase in cooling for the tropical forest zone across latitudes. Warming during the dry season was triggered by the albedo from plantation forests, but the albedo-induced forest cover change impacts on LST were quite complex. Meanwhile, ET dominated the cooling during the wet season and warm season. Additionally, enhanced precipitation played a more prominent role in the ET-induced cooling. Evaluation of the effect of temperature change induced by afforestation illustrates the importance of protecting natural forests and avoiding extensive artificial afforestation, especially in northern Guangdong Province, and reverting agricultural land to forest, especially in western Guangdong Province. This analysis also provides a basis for feedback from forest management activities to climate change in southern China.

1. Introduction

Forest cover change (e.g., afforestation) has been deemed a key strategy for climate-change mitigation. Afforestation can mitigate the effect of climate warming by triggering the climate effects of land-use through changes to the radiative (i.e., albedo) and non-radiative (i.e., evapotranspiration (ET) and surface roughness) physical states of the land surface via biophysical processes (Alkama and Cescatti, 2016; Betts, 2001; Bonan, 2008; Forzieri et al., 2017; Jackson et al., 2008; Swann et al., 2012).

Land surface temperature (LST) is a key variable for measuring environmental changes (e.g., soil, hydrology, biology, and geochemistry) of the underlying surface resulting from the physical and chemical processes associated with changes to the surface energy balances (Deng et al., 2018; Justice et al., 1998; Li et al., 2013; Liu et al., 2019; Tomlinson et al., 2011). For example, depending on the specific

* Corresponding author at: Department of Forest Resources Management, College of Forestry, Longpan Road 159, Nanjing Forestry University, Nanjing, Jiangsu Province, China.
E-mail address: nfulms@njfu.edu.cn (M. Li).

https://doi.org/10.1016/j.agrformet.2019.107641
Received 1 April 2019; Received in revised form 4 June 2019; Accepted 25 June 2019
Available online 01 July 2019
0168-1923/

vegetation change that is controlled by biophysical mechanisms (i.e., ET and albedo) and background climate (i.e., precipitation and snow), warming or cooling can occur (Duveiller et al., 2018; Pal and Ziaul, 2017). Warming reductions of afforested areas are over 3 times higher in the tropics than in the boreal and northern temperate regions (Arora and Montenegro, 2011). China has the largest afforested area in the world (˜69 million ha in 2013), accounting for approximately 33% of the global afforested area and contributing most of the carbon sinks (CSF, 2014). Southern China, specifically, accounts for 66% of the forest carbon sink (Piao et al., 2009). This is especially for the afforestation of wood products or destruction of natural forests that result in frequent spatiotemporal changes of plantation forests (CSF, 2014). However, there is limited understanding of how the biophysical effects of frequent spatial changes of afforestation (such as increased areas of fast-growing and high-yield plantation forests) attribute to the local or regional temperature in southern China.

To understand temperature responses of forests, climate models or fixed observations have previously been investigated (Arora and Montenegro, 2011; Bonan, 1997; Swann et al., 2012). Remotely sensed observation-based studies have been successful in combining the forest cover data with land surface products to monitor temperature changes at global, national, or even latitudinal scales (Jackson et al., 2008; Li et al., 2016, 2015; van Leeuwen et al., 2011). The Landsat or the Advanced Space-borne Thermal Emission and Reflection Radiometer (ASTER)-based land surface temperature (Ndossi and Avdan, 2016; Sobrino et al., 2004) has higher spatial resolution than the Moderate-Resolution Imaging Spectroradiometer (MODIS). MODIS data, however, has been widely used due to their greater temporal resolution and abundant products (e.g., MODIS albedo, ET, LST, and land cover) (Geng et al., 2014; Song et al., 2018).

The coarse-resolution MODIS forest cover data cannot adequately reflect the actual ground cover types at local scales (Coppin et al., 2004). The Landsat-based National Land Cover Database (NLCD) (Homer et al., 2007), Global Forest Change (GFC) data (Hansen et al., 2013), and fractal vegetation cover (FVC) (Pal and Ziaul, 2017) were selected for detecting LST change due to forest cover changes (Li et al., 2016; Wickham et al., 2013, 2012). The NLCD cannot be used outside the U.S., however, and the choice of threshold values used in detecting forest cover change based on GFC or FVC will influence the magnitude of the forest change impacts on temperature (Alkama and Cescatti, 2016; Li et al., 2015). Moreover, Brown et al. (1986) suggested monitoring the distribution of afforested areas with a time series of remotely sensed data for a span of 50 years. Using this approach, a more explicit spatiotemporal pattern of abrupt and gradual forest cover changes could be obtained (Banskota et al., 2014; Shen et al., 2019) compared with traditional sample plot survey data (Zeng et al., 2015). Integration of optical sensors (e.g., Landsat and Landsat-like sensors), as well as Synthetic Aperture Radar sensors (SAR) (e.g., Phased Array L-band Synthetic Aperture Radar (PALSAR) on the Advanced Land Observing Satellite (ALOS)) has been shown to be useful in understanding the spatial distribution of time series forest cover changes associated with afforestation (Shen et al., 2019), due to their similar pixel size and multi-temporal features (Shen et al., 2019). However, we still have a limited knowledge of the effects of combining Landsat and PALSAR-based land cover data and MODIS-based land surface products in order to monitor the biophysical processes of plantation forests change and its effect on land surface temperature.

Some researchers have used the moving window method at the sample grid cell level to determine the impact of forest change on LST (Alkama and Cescatti, 2016; Li et al., 2015; Peng et al., 2014; Wickham et al., 2012). This method has been used with either a single-year land cover map or a forest cover map (Li et al., 2015; Wickham et al., 2013, 2012), as well as multiyear forest change maps (Tang et al., 2018). These studies, however, did not explore the climatic effects of the specific forest management practices (e.g., afforestation and reforestation). The spatial investigation method of the time series analysis at the pixel level has also been used to separate the temperature effects of multiple types of land cover transitions (Zhang and Liang, 2018). However, few studies have directly investigated the effects of individual year and multiyear forest cover change due to afforestation and reforestation in the southern plantation forest region on spatiotemporal LST change using previous remote sensing-based methods in combination with *in situ* measurements (i.e., air temperature and precipitation).

The specific objectives of the current study were to: (1) quantify the spatiotemporal change pattern of plantation forests (PF); (2) explore the hypothetical change (year 2010) and actual change (2000–2010) effects of the conversion of natural forests (NF) and open lands (grassland (GR) and cropland (CR)) to plantation forests on land surface temperatures; and (3) understand the driving effects of albedo, ET, air temperature and precipitation in conjunction with afforestation changes from 2000 to 2010 on land surface temperature in Guangdong Province, southern China.

2. Materials and methods

2.1. Study area

The study area was located in Guangdong Province, China (20°13′N–25°31′N, 109°39′E–117°19′E, 17.97×10^4 km^2, Fig. 1). The elevation of this region ranges from 22 to 1353 m above sea level. The latitudinal climate varies from subtropical (mid-subtropical and south-subtropical) to tropical with 3 forest zones called: mid-subtropical typical evergreen broadleaved forests ("Mid-subtropical forest zone"), south-sub-tropical monsoon evergreen broadleaved forests ("South-subtropical forest zone"), and tropical monsoon forest or rainforest ("Tropical forest zone") (Shen et al., 2018) (Fig. 1). The annual mean precipitation is 1300–2500 mm, and the temperature ranges from 19 to 24 °C. Guangdong is wet from April to September, arid from November to January, and the other months are transitional (Shen et al., 2018). The dominated trees are *Pinus massoniana, Cunninghamia lanceolata, Schima superba, Eucalyptus urophylla, Eucalyptus robusta, Pinus elliottii, and Hevea brasiliensis.* There are three crops per year, such as double cropping of rice and one other crop. Northern and western Guangdong have the largest distribution of forests and croplands, respectively (CSF, 2014).

2.2. Data used and data pre-processing

2.2.1. Forest cover datasets

Annual forest/non-forest products (1986–2016) based on the "SGB-NDVI" algorithm (SGB-NDVI-based FNF) was generated by combining the Landsat-based phenological variables with PALSAR-based land cover classifications (Shen et al., 2019). The forest accuracy ranged from 79% to 85% and the non-forest accuracy range from 91% to 95% (Shen et al., 2019) (Table 1). Grassland, cropland, and forest types were generated from China's 30 m global land cover (GlobeLand30) (Chen et al., 2015) for the years 2000 and 2010. The user accuracy of forest, grassland, and cropland was 84% (89%), 77.5% (76.88%), and 85.1% (83.06%), respectively, for the GlobeLand30 in 2000 and 2010, and the overall accuracy of two GlobeLand30 datasets for years 2000 and 2010 was > 80% (Chen et al., 2015) (Table 1). The overall data processing and analysis workflow is summarized in Fig. 2.

2.2.2. MODIS land surface data

Land surface temperature data (MYD11A2, EOS-Aqua-MODIS) from 2002 to 2018 was used (Table 1) (Wan, 2008). Aqua-based overpass time was closer to the lowest and highest temperatures during the day. Due to the fact that the land surface temperature tends to increase as the day progresses and is affected by water stress, overpass time from the afternoon tends to be more useful for capturing the effects of afforestation (Mildrexler et al., 2011). The LST data include daytime (˜13:30 PM from Aqua) and nighttime (˜01:30 AM from Aqua)

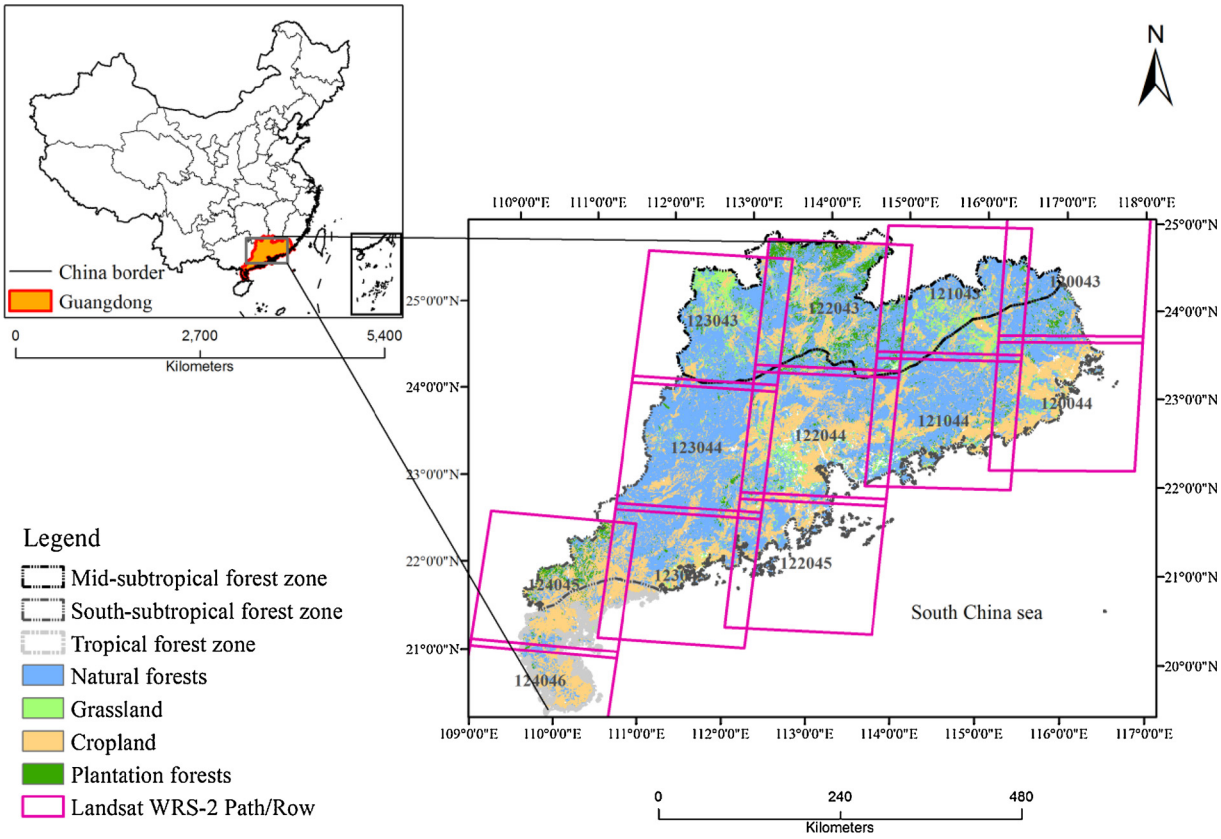

Fig. 1. Overview of the study area in Guangdong Province, China. The background land cover map is from 2010, including plantation forests, natural forests, grassland, and cropland (the number "122043" is a Landsat Path/Row). Dashed lines show 3 climate-based forest zones from north to south: mid-subtropical, south-subtropical, and tropical.

temperature observations under clear sky; no cloud effects were selected (the emissivity error < 0.02, and the LST error < 1 K, Wan (2008)). All of the data (units: K) were converted to degrees Celsius (°C).

We used the new ET (MOD16A2.105_MERRAGMAO) product collected from Numerical Terradynamic Simulation Group (NTSG) (University of Montana), spanning from 2000 to 2014 (Table 1) (Mu et al., 2011). The albedo (MCD43B3v005) product developed by the MODLAND group from 2000 to 2017 was selected (Table 1) (Schaaf et al., 2002). The use of black sky albedo (BSA) to represent the true albedo is recommended by the FAO report (www.fao.org/gtos/doc/ECVs/T08/GTOS-ECV-T08-albedo-v11.pdf). Here, short-wave BSA (0.3–5.0 μm) was extracted and used and we ensured that the albedo data error was less than 5% (Liu et al., 2009).

All of the data with HDF-EOS and Sinusoidal projection were batching extracted and converted to longitude and latitude coordinates (WGS84) using the function gdalwarp.py from the GDAL library (http://www.gdal.org/). First, multiyear average values of all of the products were calculated at an 8-d scale. Second, results were further average by month of the season (winter = December, January, February; spring = March, April, May; summer = June, July, August; autumn = September, October, November). They were also averaged by year for daytime LST, nighttime LST, ET, and albedo. In order to quantify the LST changes, the LSTs, ETs, and albedos from 2000, 2001, 2002, and 2003, were averaged to represent the LST, ET, and albedo around 2000, while the average values from 2007, 2008, 2009, and 2010 represented the LST, ET, and albedo around 2010.

2.2.3. Climate data

Annual maximum and minimum temperature and precipitation averages were collected from the 26 meteorological stations across Guangdong Province for 2000 and 2010. The annual averages for these years were obtained from the China Meteorological Administration annual ground dataset (1952–2016). We developed a random forest (RF) model to perform spatial interpolation of air temperature and precipitation. Critical variables, such as latitude, longitude, and elevation, were used in the model. The remaining 20% of samples were reserved for assessing the interpolation accuracy of the model using the independent validation data set approach. We calculated Pearson's correlation coefficients (r), the slope, and the intercept of linear regression lines for meteorological station data (observed values) versus interpolated results (predicted values), root mean square deviation

Table 1
Summary of satellite-based products used in this study, including 2 land cover products, MODIS-based LST, ET, and albedo products.

Data set	Type	Resolution	Time period	Tile	Reference
SGB-NDVI-based FNF	Forest/nonforest	30 m	1986–2016	12paths/rows (Fig. 1)	(Shen et al., 2019)
China's GlobeLand30	Land cover types	30 m	2000, 2010	12paths/rows	(Chen et al., 2015)
MYD11A2 (Aqua)	LST	1km, 8days	2002–2018	h28v06	(Wan, 2008)
MOD16A2.105	ET	1km, 8days	2000–2014	h28v06	(Mu et al., 2011)
MCD43B3	Albedo	1km, 8days	2000–2017	h28v06	(Schaaf et al., 2002)

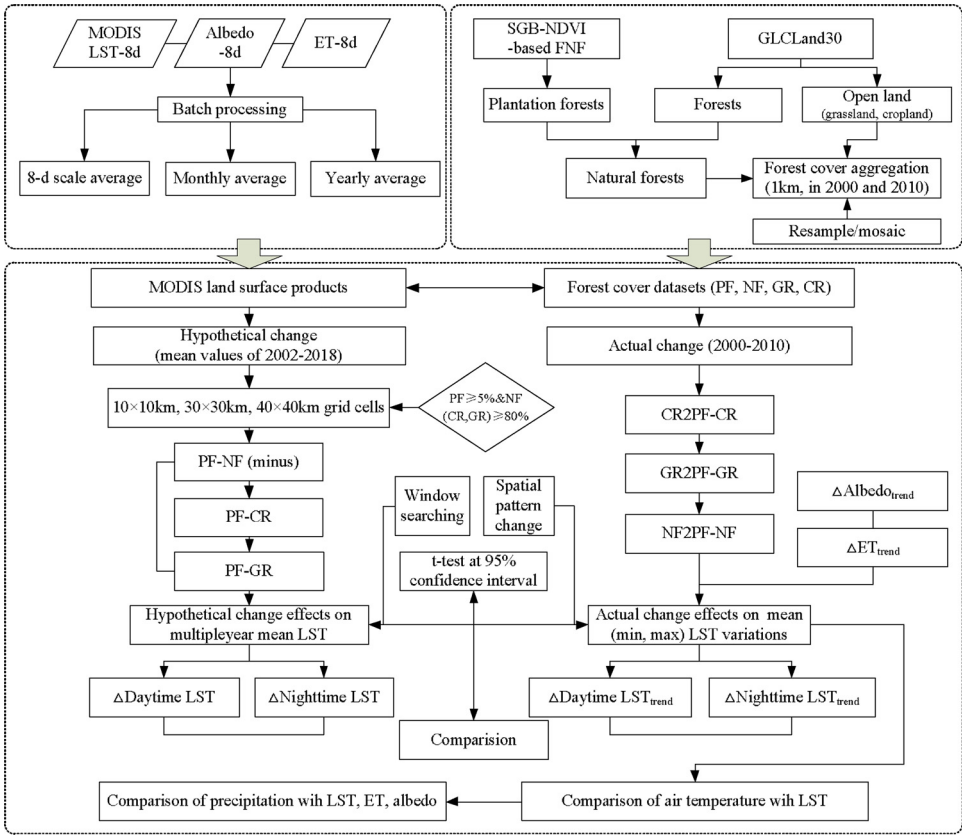

Fig. 2. Workflow diagram.

(RMSD), and the out of bag model error as a function of the number of trees.

2.2.4. Topographic data

Topography variables from the NASA Shuttle Radar Topographic Mission (SRTM) digital elevation model (DEM) data were re-projected from 30 m resolution to 1 km spatial resolution with nearest neighbor resampling. By constructing the linear regression equation between temperature variations and the corresponding elevation variations, the elevation adjustment was conducted to offset the temperature biases due to elevation differences (Li et al., 2015).

2.3. Identification of plantation forests and open lands

Artificial afforestation and reforestation were considered as the remote sensing-based plantation forests (Brown et al., 1986). Here, a spatial pattern map of plantation forest (e.g., 2010) was generated as the intersection between non-forest from the year before the current year (i.e., persisting non-forest or deforestation in 2009) and the forest in the current year (i.e., afforestation or post-deforestation reforestation in 2010) based on SGB-NDVI-based FNF (Shen et al., 2019). Open lands were extracted from non-forests, which may have resulted from deforestation or may be suitable for future afforestation and reforestation (Lee et al., 2011). Next, two forest cover datasets (plantation forest and non-forest), and GlobeLand30-based grassland, cropland, and forest (Chen et al., 2015), were aggregated into new datasets that included plantation forests, natural forests, and open lands (grassland and cropland) in the years 2000 and 2010 (Fig. 1). These data were resampled from 30 m resolution to 1 km spatial resolution with nearest neighbor interpolation to make them consistent with the MODIS land surface data (Fig.2).

2.4. Analysis of LST induced by the hypothetical PF change

The hypothetical change of plantation forests refers to a forest change that is a hypothetical concept and has yet to occur in reality, as all of the changes take place within the same sample grid cells in a single year. Sample grid cells measuring 10 × 10 km, 30 × 30 km, and 40 × 40 km and covering the study area were selected to quantify change in the aggregated plantation forests, natural forests, cropland, and grassland dataset in 2010 (Fig. S1). The rules that there must be at least 5% cover of plantation forests and over 80% cover of natural forests or open land in every sample gird cell were followed to further filter grid cells on the aggregated 1 km spatial resolution forest cover map. The multiyear mean LST, ET, and albedo differences (2002–2018) of forests minus open lands were calculated based on the window searching method (Li et al., 2015) at the sample grid cell level for hypothetical change (Fig. S1, Method 1). The impacts of plantation forests on local temperature were expressed as the LST difference (ΔLST) of plantation forests minus open lands following Eq. (1):

$$\Delta LST = LST_{\text{plantation forests}} - LST_{\text{open lands}} \quad (1)$$

Positive and negative ΔLST indicate warming and cooling effects of plantation forests, respectively. Zero values indicate no significant difference.

2.5. Analysis of LST change induced by the actual PF change

The actual afforestation change can be identified as a transition from other forest and non-forest types to plantation forest, with all of the changes occurring at the pixel level within a given time period. Due to the limited time series for MODIS products and the abundance of land cover products in 2000 and 2010, we explored the difference in LST from 2000 to 2010 to quantify the actual change trend. This was based on the temporal-spatial pattern change analysis method (Fig. S2).

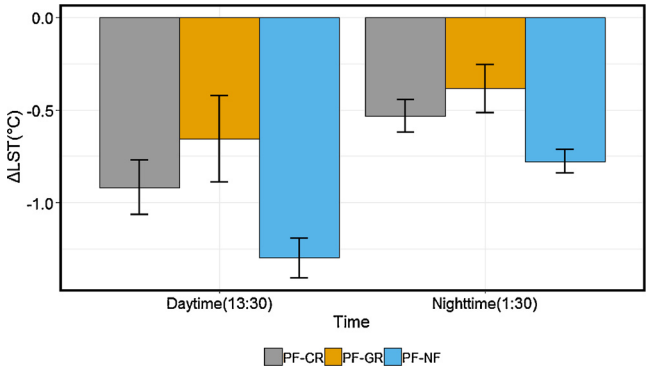

Fig. 3. The annual mean land surface temperature difference of plantation forests minus natural forests (cropland and grassland) during the daytime (˜13:30 PM) and nighttime (˜01:30AM). Measurements are from a 10 × 10-km grid size in Guangdong Province, China, from 2002 to 2018. The vertical lines on each bar represent the confidence interval at 95% estimated by *t* test.

The effects of spatial changes in plantation forests on the surface temperature can be determined by calculating the LST difference between the periods of the changing plantation forests pixels (i.e., afforestation) and the starting year changed non-forest pixels (open lands) or other forests pixels (i.e., natural forests). The monthly and yearly difference in change of daytime and nighttime LST, ET, and albedo between plantation forests and grassland or cropland from 2000 to 2010 can be represented using Eq. (2) (CI is estimated by *t* test at 95%) (Fig. S2, Method 2).

$$\Delta LST_{trend} = LST_{\text{open lands transfers to plantation forests}} - LST_{\text{open lands}} \quad (2)$$

For example, the positive ΔLST_{trend} represents a warming effect of plantation forests, while negative values imply a cooling effect, and zero values imply no significant difference. The relationship between ΔLST_{trend} and $\Delta albedo_{trend}$ or ΔET_{trend} were evaluated using the monthly mean of the above difference values to fit linear regression models. Next, albedo and ET transition data were divided by various time periods to extract and analyze statistical information (mean, median, the lower and upper 25 percentiles, and maximum and minimum values) from the changed temperature data between PF, natural forests, CR, and GR.

2.6. Analysis of the relationship between air temperature and LST associated with PF change

The trend of air temperature change (2000–2010) can also be defined by Eq. (2) and analyzed using the same methods as Fig. S2. We compared the temperature change trends between annual average maximum and minimum air temperature and daytime and nighttime LST. The relationships between the air temperature values from the interpolated grid datasets and LST (daytime and nighttime) were validated using a linear regression and estimated by adjusted R square (R^2_{adjust}), slope, and intercept.

2.7. Analysis of the contribution of precipitation to LST associated with PF change

The change trend of precipitation for 2000–2010 can be defined by Eq. (2) and analyzed in the same way as Fig. S2. We validated the linear regression relationships for the different precipitation values from the interpolated grid datasets and ET or daytime temperature, nighttime temperature, and albedo. The precipitation transition was subdivided into various time periods in order to better understand the relationship between precipitation and ET or temperature and albedo.

3. Results

3.1. Assessment of the spatiotemporal pattern of plantation forests maps

Based on the national forestry year book of China, the forest area in Guangdong consisting of a plantation forest (4.41×10^6 ha and 5.03×10^6 ha) increased by 0.62×10^6 ha from 2000 to 2010. Meanwhile, this increase was 0.60×10^6 ha in the current study. This inconsistency was due to the differentiated definition of the plantation forests. The validation of the plantation forests maps was not easily generated, and therefore, the accuracy of the 2 forest cover products discussed in section 2.2.1 has been recognized as one of the validation results of the plantation forests maps.

3.2. Effects of yearly (seasonal) hypothetical change of PF on latitudinal variation-based LST

The total number of sampled grid cells for the hypothetical change comparison between: PF and NF, GR, and CR in the 10 × 10 km area (Fig. 4), 30 × 30 km area, and 40 × 40 km area (Fig. S3), respectively, were selected. A 10 × 10 km in size had 1797 grid cells (66, 67, and 21 sampled grid cells for calculating the differences between PF and NF, CR, and GR, respectively) (Fig. S3).

Afforestation in 2010 reduced the 2002–2018 multiyear means of the daytime and nighttime surface temperatures from the 3 different sample window sizes (Fig. S4). Here, detailed statistical measurements were performed using 10 × 10-km sample grids (Fig.S3). It was found that the temperature difference (ΔLST) of PF minus NF was relatively large (Fig. 3). The average temperature differences of PF minus NF, as well as PF minus CR, were greater than that of PF minus GR. In particular, the daytime temperature difference (0.64 ± 0.13 °C and 0.26 ± 0.08 °C) for PF and NF or CR was greater than that between PF and GR. The nighttime temperature difference (0.39 ± 0.07 °C and 0.14 ± 0.04 °C) of PF minus NF (CR) was also higher than PF minus GR, based on the 10 × 10-km grid size ($P < 0.05$, Student's *t* test) (Fig. 3). Overall, afforestation reduced temperatures more during the day than at night (Fig. 3). Afforestation reduced the multiyear average surface temperature from 2002 to 2018 by 0.76 ± 0.13 °C. The mean daytime temperature dropped by 0.95 ± 0.16 °C, and the mean nighttime temperature dropped by 0.57 ± 0.09 °C.

Fig. 4 shows that the temperature difference of plantation forests minus open land during the daytime and nighttime was greater in summer (i.e., June–August) than in the winter (i.e., December–February). The average temperature difference of plantation forests minus cropland was greater than that of plantation forests minus grassland. For example, the temperature difference was –0.27 ± 0.12 °C (daytime) and –0.18 ± 0.07 °C (nighttime) in summer for the 10 × 10-km grid size. We found similar trends for a larger sample grid (30 × 30 km or 40 × 40 km) (Fig. S5). Generally, cropland replaced by afforestation decreased the temperature during the daytime and nighttime, but the daytime experienced the most cooling. Therefore, there was a strong net cooling effect of afforestation.

Hypothetical changes associated with afforestation in 2010 in the tropical forest zone had a stronger cooling effect than other forest zones, especially during the daytime. There was a slight discrepancy in the effects of the LST difference of PF minus NF (Fig. S6). Afforestation of natural forests caused the greatest drop in multiyear average temperature, whereas there was no decrease for grassland converting to plantation forests in the south-subtropical forest zone (Fig. S6).

Fig.S7 illustrates the same seasonal variation trends of the multiyear mean daytime or nighttime temperatures for LST induced by the hypothetical changes of nearby land cover types converting to PF in 2010, even though in the different forest zones with monthly estimation in Fig. 4, greater cooling in summer than in winter was found. The latitudinal variation for the multiyear mean daytime and nighttime LST was consistent with that in Fig. S6. In the summer, we observed a

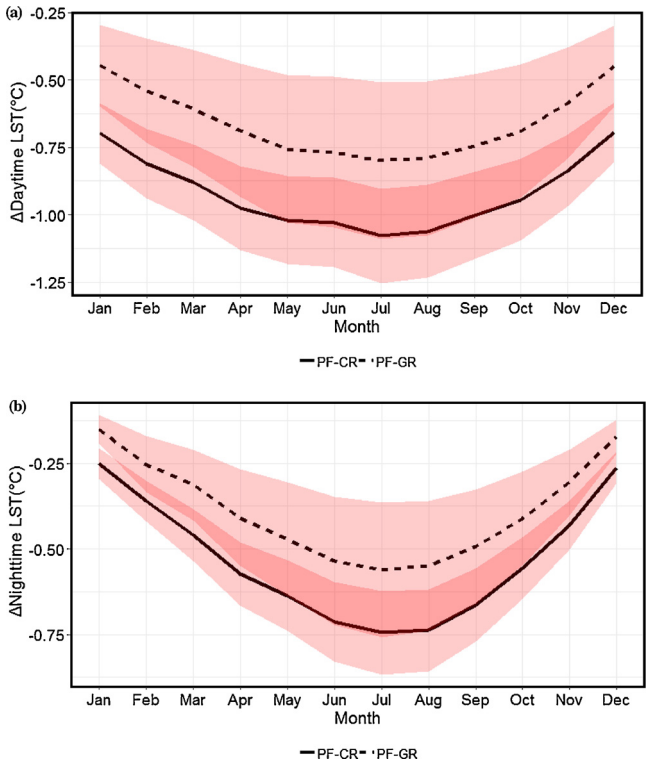

Fig. 4. Monthly daytime (a) and nighttime (b) land surface temperature differences of plantation forests minus cropland (grassland) in Guangdong Province, China, for a 10 × 10-km area. The red shaded area represents the confidence interval at 95% estimated by the Student's *t* test (For interpretation of the references to colour in this figure legend, the reader is referred to the web version of this article).

similar cooling effect for afforestation of cropland during for tropical and mid-subtropical forests. In the winter, the hypothetical changes associated with afforestation in the mid-subtropical forest zone showed no noticeable cooling compared with that in the southern forest zone or tropical forest zone during the nighttime, illustrating the latitudinal variations in cooling from north to south.

3.3. Actual change of plantation forest and its impacts on temperature change (2000–2010)

Fig. 5 shows the spatial distribution pattern of actual changes between plantation forests, natural forests, cropland, and grassland, and their impacts on daytime LST, nighttime LST, ET, and albedo from 2000 to 2010. Values were derived from the changes from 2000 to 2010 minus the non-change open lands or natural forests in 2000 at the pixel level. In particular, there were large areas of transition from natural forests and croplands to plantation forests in northern and western Guangdong during this time, respectively (Fig. 5a). Obvious changes in annual daytime LST, nighttime LST, ET, and albedo from cropland, grassland, and natural forests that became plantation forests have been detected. LST decreased significantly (Fig. 5b and Fig. 5c), especially daytime LST (Fig. 5b) when croplands were converted to plantation forests. A slight daytime LST increase was observed for the areas which grasslands and natural forests transitioned to plantation forests, especially in northern Guangdong (Fig. 5b). Moderate changes in albedo and ET were derived in areas with afforestation (Fig. 5d and e).

3.3.1. Effects of PF changes on yearly and seasonal variation-based LST change

The annual afforestation change of cropland from 2000 to 2010 had a cooling effect on the mean daytime and nighttime temperature. Grassland and natural forests had a slight warming effect on the mean daytime temperature. Overall, daytime warming caused by the difference between PF and GR, and PF and NF was offset by daytime cooling caused by PF and CR. Moreover, daytime warming and nighttime cooling between PF and NF was balanced (ΔLST_{trend}~0 °C), and therefore, there was almost no difference in annual temperatures of PF minus NF. Therefore, there was a consistent cooling effect (–0.22 ± 0.02 °C) during the daytime which was greater than nighttime (–0.13 ± 0.03 °C) (Fig. 6).

Fig. S8 illustrates the cooling effect caused by the mean temperature difference of PF minus CR from 2000 to 2010, which was more pronounced than other changes. The seasonal difference was assessed, and in the winter and autumn, the difference due to afforestation changes in daytime LST consisted of a warming effect of 0.75 ± 0.08 °C and 0.47 ± 0.06 °C, and in summer and spring, it consisted of a cooling effect of approximately –0.32 ± 0.08 °C and –0.97 ± 0.13 °C (Fig. S8a). In the winter, summer, and autumn, the nighttime LST difference produced warming effects of about 0.39 ± 0.09 °C, 0.17 ± 0.05 °C, and 0.36 ± 0.04 °C, respectively. In the spring, it produced a cooling effect of about –1.38 ± 0.1 °C (Fig. S8b). Nighttime warming in the summer was offset by daytime cooling; thus, the LST difference caused by afforestation in the summer decreased by 0.15 ± 0.03 °C. Meanwhile, a greater increase in warming was detected during the day than at night in the winter, illustrating a warming effect. Overall, the difference in cooling due to afforestation in the spring balanced changes in other seasons, and resulting in a net cooling effect.

In regard to whether conditions were dry or wet, daytime warming of 0.33 ± 0.05 °C was detected during the dry season and daytime cooling of –0.46 ± 0.09 °C was detected during the wet season, inducing a cooling effect due to actual afforestation changes (Fig. S8a). Conversely, there was a nighttime cooling effect during the dry season (–0.42 ± 0.05 °C) and wet season (–0.49 ± 0.05 °C) (Fig. S8b). We conclude that with more precipitation, more cooling occurred, and that in the dry season when it was cool at night and warm in the day, daytime warming was offset by nighttime cooling from 2000 to 2010.

3.3.2. Seasonal effects of PF changes on latitudinal variation-based LST change

Although a cooling effect due to the actual afforestation changes from 2000 to 2010 was detected, there was a pronounced temperature change difference between climatic-based forest zones; latitudinal variations from north (mid-subtropical forest zone) to south (tropical zone) also occurred. Actual afforestation changes in the mid-subtropical forest zone had a warming effect (0.42 ± 0.05 °C) during the daytime, particularly for natural forests moving to plantation forests. Still, afforestation changes in the tropical forest zone had a cooling effect of –0.78 ± 0.14 °C and in the south-subtropical forest zone of –0.51 ± 0.07 °C. South-subtropical forests were ranked second, due to the fact that the difference between PF and CR was the largest (Fig. 7a). The greatest cooling associated with PF changes in the tropical forest zone occurred at night (–0.3 ± 0.07 °C), followed by south-subtropical forest zone (–0.23 ± 0.04 °C), and mid-subtropical forest zone (–0.04 ± 0.03 °C). Meanwhile, a negligible warming of 0.003 ± 0.04 °C was offset by cooling between PF and CR (Fig. 7b).

In the winter, the actual PF changes in the mid-subtropical forest zone, south-subtropical forest zone, and tropical forest zone resulted in a daytime warming of 0.92 ± 0.11 °C, 0.64 ± 0.13 °C, and 0.09 ± 0.29 °C, respectively, (Fig. 8a). Nighttime warming of 0.56 ± 0.13 °C and 0.18 ± 0.12 °C was detected for PF changes in the mid-subtropical and south-subtropical forests. The inverse was that afforestation in the tropical forest zone had a cooling effect of about –0.24 ± 0.23 °C (Fig. 8b). On average, there was a warming effect in winter, but it was reduced as the latitude moved from north to south. In the summer, afforestation changes in all of the climate-based forest zones from north to south resulted in cooling in the daytime, with respective temperature changes of –0.1 ± 0.09 °C, –0.61 ± 0.13 °C, and

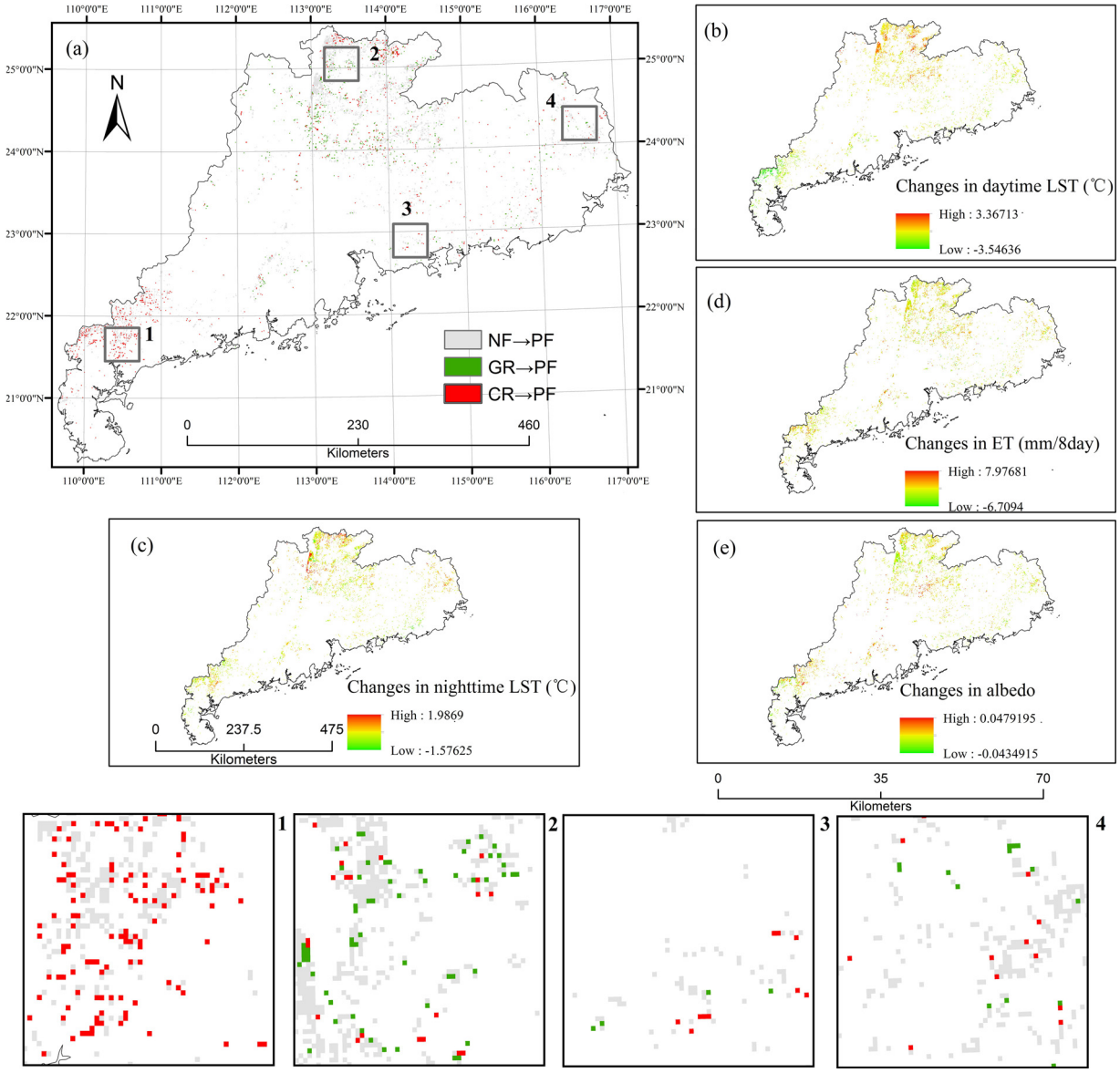

Fig. 5. Changes (a) in open land (CR and GR) and natural forests (NF) to plantation forests (PF) of (b) annual daytime LST (ΔDaytime LST_{trend}); (c) Nighttime LST (ΔNighttime LST_{trend}); (d) ET (ΔET_{trend}); (e) Albedo ($\Delta Albedo_{trend}$) in Guangdong Province, China, from 2000 to 2010. Four zoomed-in maps present more detailed views of land use change.

–0.21 ± 0.36 °C (Fig. 8a). The corresponding changes in nighttime warming were 0.16 ± 0.07 °C, 0.14 ± 0.07 °C, and 0.41 ± 0.13 °C (Fig. 8b). In fact, the summer temperature showed a cooling effect caused by diurnal variation, along with a trend of warming to cooling, and then finally warming across latitudes.

3.3.3. *Biophysical impacts of PF changes on spatiotemporal variation-based LST changes*

The annual mean albedo difference ($\Delta Albedo_{trend}$) due to afforestation change from 2000 to 2010 was 0.004 ± 0.0003 (Fig. 9a). Although the mean albedo difference values were positive, they were so low as to be almost negligible, leading to a cooling effect. However, Fig. 10 shows that the albedo difference values were < 0, indicating a cooling effect, whereas those were > 0 indicating a warming effect during the daytime. This does not agree with previous observations that there should be a warming effect due to the fact that forests generally have low albedo and absorb large amounts of incoming solar radiation. Thus, albedo variations alone might not determine the temperature change (Fig. S9). The annual mean ET difference (ΔET_{trend}) was about 0.43 ± 0.06 mm per 8 d, especially between PF and GR (Fig. 9b). The ET had a negative correlation with the trend of daytime LST, leading to a cooling effect (Fig. S9). This was due to the high ET in plantation forests. Fig. 10c shows that mean ET difference values were > 0, indicating a cooling effect during the daytime, as well as nighttime.

Fig. 11 shows the negative mean albedo change values in the spring season. The differences in ET generally showed that plantation forests had a higher ET than other forest or non-forest types, especially in the summer, followed by autumn, although winter was the opposite (Fig. 11). Moreover, a higher ET in plantation forests (particularly GR converting to PF) during the wet season was detected (Fig. 11).

The actual afforestation changes in the south-subtropical forest zone resulted in the greatest positive albedo (ET) values, while those in the tropical forest zone were associated with the least negative albedo (positive ET) values (Fig. S10 and Fig. S9). In the summer, the albedo difference (values in the tropical forest zone were negative) increased across the latitudes, whereas the ET (values were positive) decreased from the mid-subtropical to the tropical to south-subtropical forest zone (Fig. S11). In the winter, the albedo difference (values were positive)

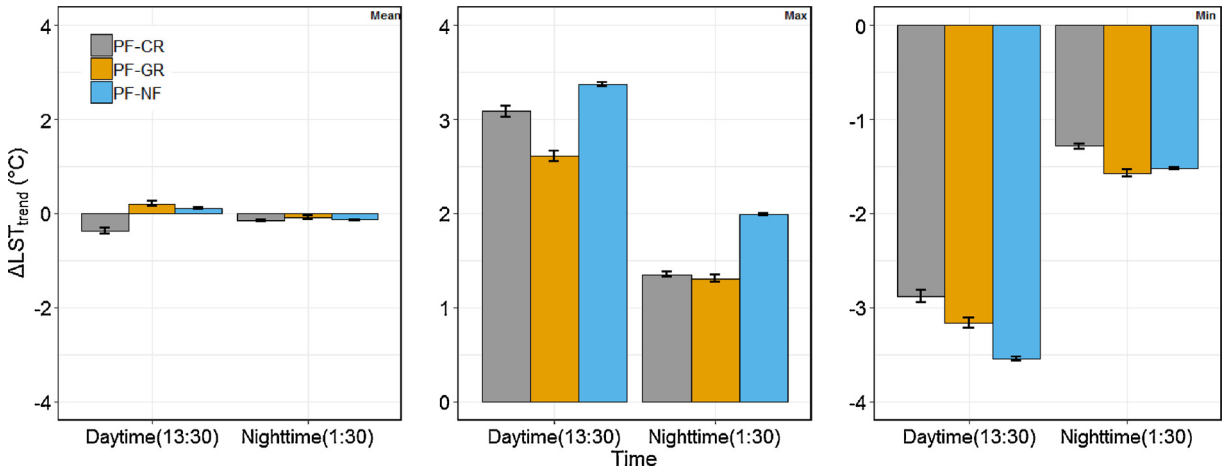

Fig. 6. Annual (mean, maximum, and minimum) land surface temperature differences (ΔDaytime LST_{trend} and ΔNighttime LST_{trend}) from 2000 to 2010 between plantation forests and the natural forests, cropland, and grassland. Measurements are for the daytime (˜13:30 PM) and nighttime (˜01:30 AM) in Guangdong Province, China. The vertical lines on each bar represent the confidence interval at 95% estimated by Student's *t* test.

increased with the latitude, while there was a decreasing ET (values were negative) across the latitudes (Fig. S11).

3.4. Comparison of LST, ET, and albedo with air temperature and precipitation

3.4.1. Validation of local meteorological station-based climate data interpolation maps

Combining the latitude, longitude, and elevation estimated climate

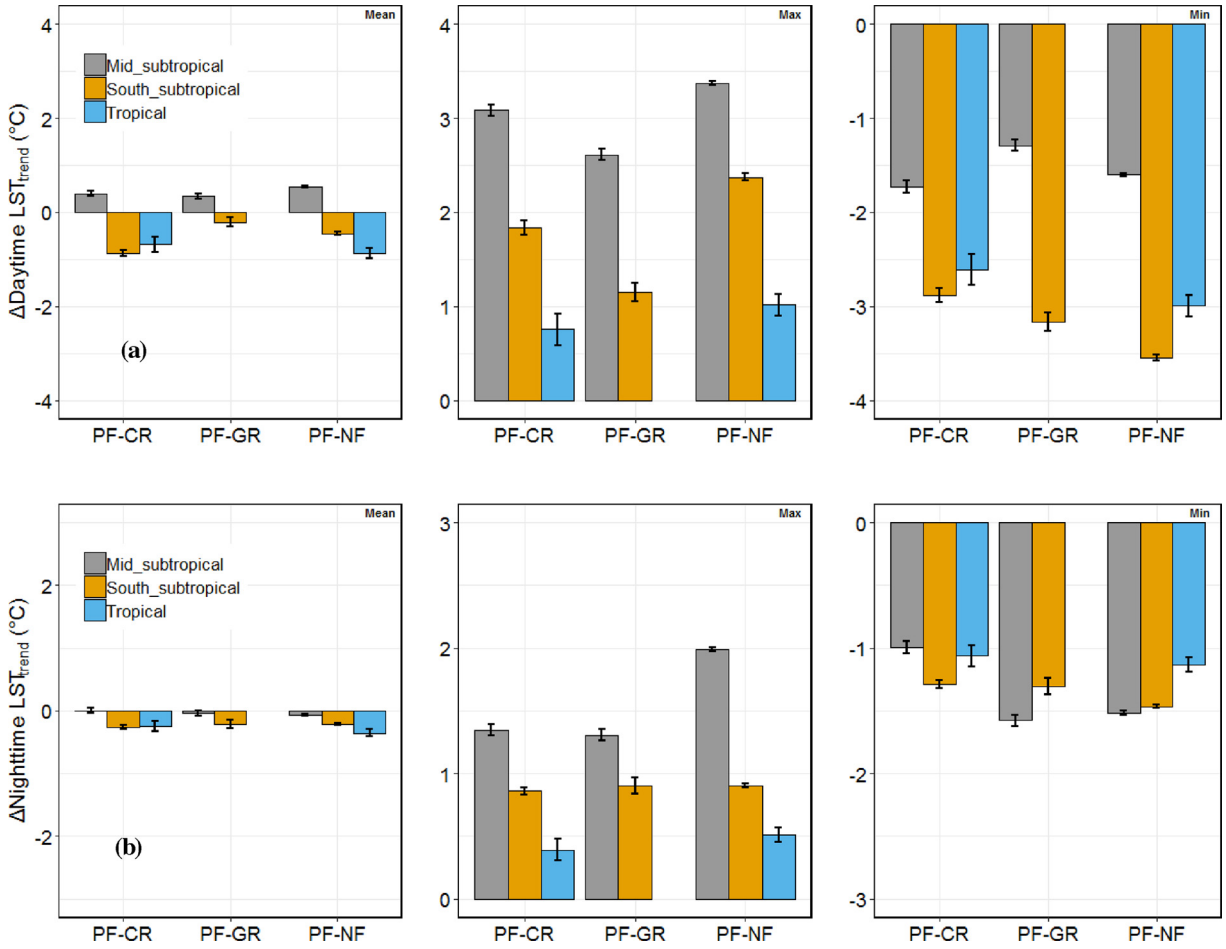

Fig. 7. Annual (mean, maximum, and minimum values) daytime (˜13:30 PM, a) and nighttime temperature (˜01:30AM, b) differences of plantation forests minus natural forests, cropland, and grassland (ΔLST_{trend}) over 3 climate zone-based forest zones, in Guangdong Province from 2000 to 2010. The vertical lines on each bar represent the confidence interval at 95% estimated by Student's *t* test.

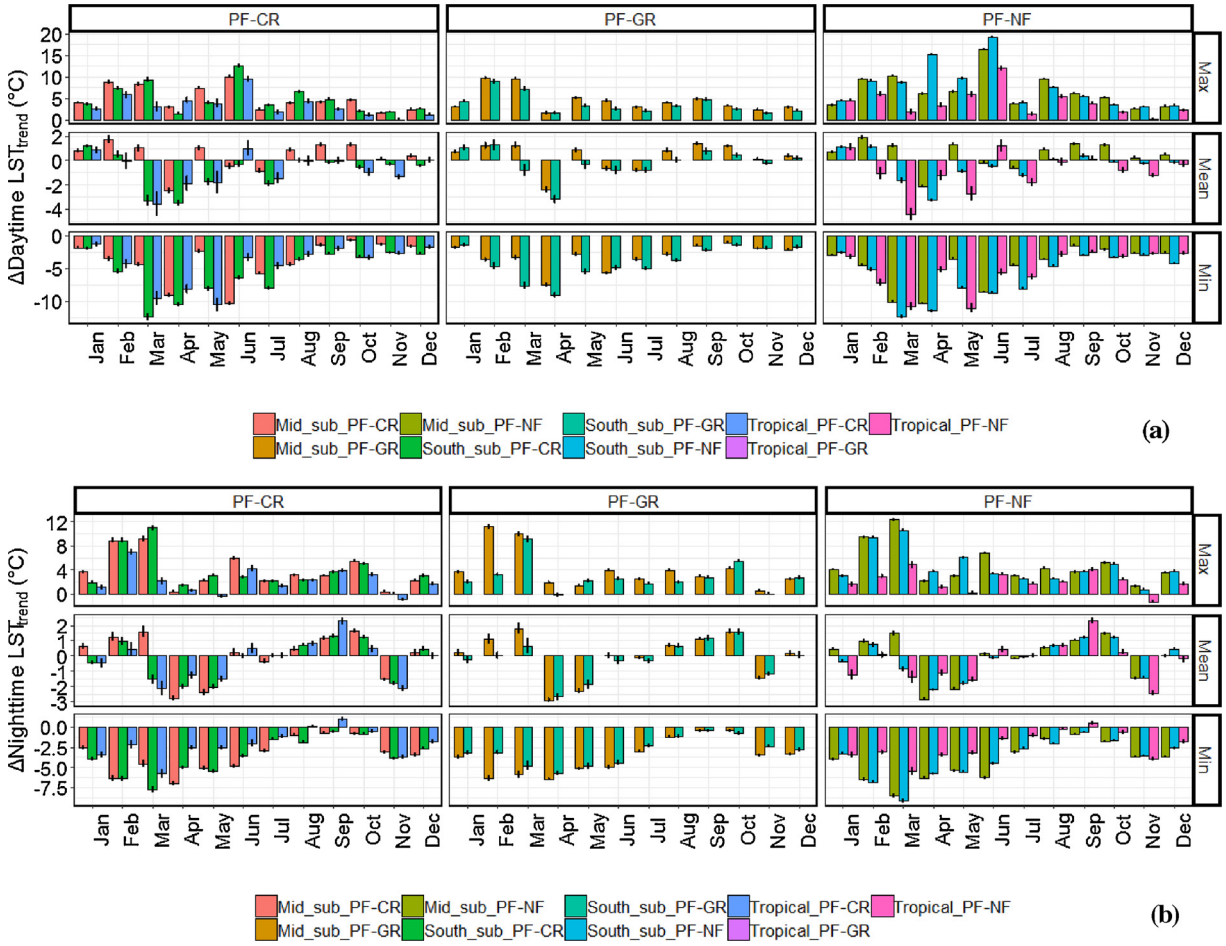

Fig. 8. Monthly (maximum, mean, and minimum) daytime (a) and nighttime (b) land surface temperature differences of plantation forests minus open land over 3 climate zone-based forest zones in Guangdong Province, China, from 2000 to 2010. The vertical lines on each bar represent the confidence interval at 95% estimated by Student's *t* test.

data (i.e., precipitation, average maximum temperature, and average minimum temperature, "pred"), we found a strong correlation with the meteorological station-based climate data ("obs") for 2000 and 2010 (R = 0.62/0.85, 0.83/0.75, and 0.99/0.98, respectively) (Table S1). These results demonstrate that the interpolated local precipitation and air temperature map had a reasonable accuracy, which can be used as an alternative to true data.

3.4.2. Relationship between air temperature and LST

Fig. S12 indicates that there was not a robust correlation between LST and air temperature associated with the actual afforestation changes from 2000 to 2010 ($0.22 < R < 0.53$, p-value < 0.001). Fig. 12 shows in terms of average air temperature, there was a cooling effect (–0.10 ± 0.02 °C) during both the daytime and nighttime. We found similar cooling effects for LST and air temperature, but the mean temperature decrease in LST (–0.18 ± 0.02 °C, Fig. 6) was larger than the air temperature.

3.4.3. Relationship between precipitation and LST, ET, and albedo

Positive (mean and median values > 0) ΔDaytime LST$_{trend}$ between PF and GR with ΔPrecipitation$_{trend}$ between 500 mm and 700 mm was detected (Fig. 13a), these results suggested that afforestation changes from 2000 to 2010 would likely lead to a warming effect, but that daytime warming was offset by nighttime cooling (Fig. 13b). The mean albedo for the afforestation region was positive, especially when precipitation increased (Fig. 13c). It may have been due to the strong albedo cooling the surface when precipitation decreased (Fig. 13a and b), however, there was not adequate evidence that albedo had a noticeable effect on temperature (Fig. S9). The mean ET for the afforestation region was positive, likely leading to cooling (Fig. 9b, Fig. S9), which can be explained by the abundant precipitation (Fig. 13d). Overall, the relationship between precipitation and LST in the afforested region from 2000 to 2010 led to a net cooling effect, due to the balance between nighttime and daytime LST (Fig. 13a and b).

4. Discussion

4.1. Analysis of hypothetical change of PF in detecting temperature

In regard to the hypothetical change effect due to afforestation in 2010, a cooling effect (0.76 ± 0.13 °C) based on the annual, seasonal, and latitudinal variations between PF and nearby lands was detected, although we did not detect a warming effect associated with changes of land cover types to PF. These results are inconsistent with findings presented by Peng et al. (2014) (˜ 0.9 ± 0.5 °C), who found that afforestation of lands south of 25 °N in China increased nighttime LST by approximately 0.1 ± 0.5 °C between PF and CR, with no significant difference in LST between PF and NF (ΔLST˜0 °C). The reason for this contradictory finding is unclear, even though we used a similar window searching method on the sample grid cells that detected hypothetical changes. Possible reasons for this inconsistency include the fact that the number of sample grids was limited and the hypothetical change from the different spatial change maps of PF in a single year may not represent the actual spatial variations. Further studies are required to

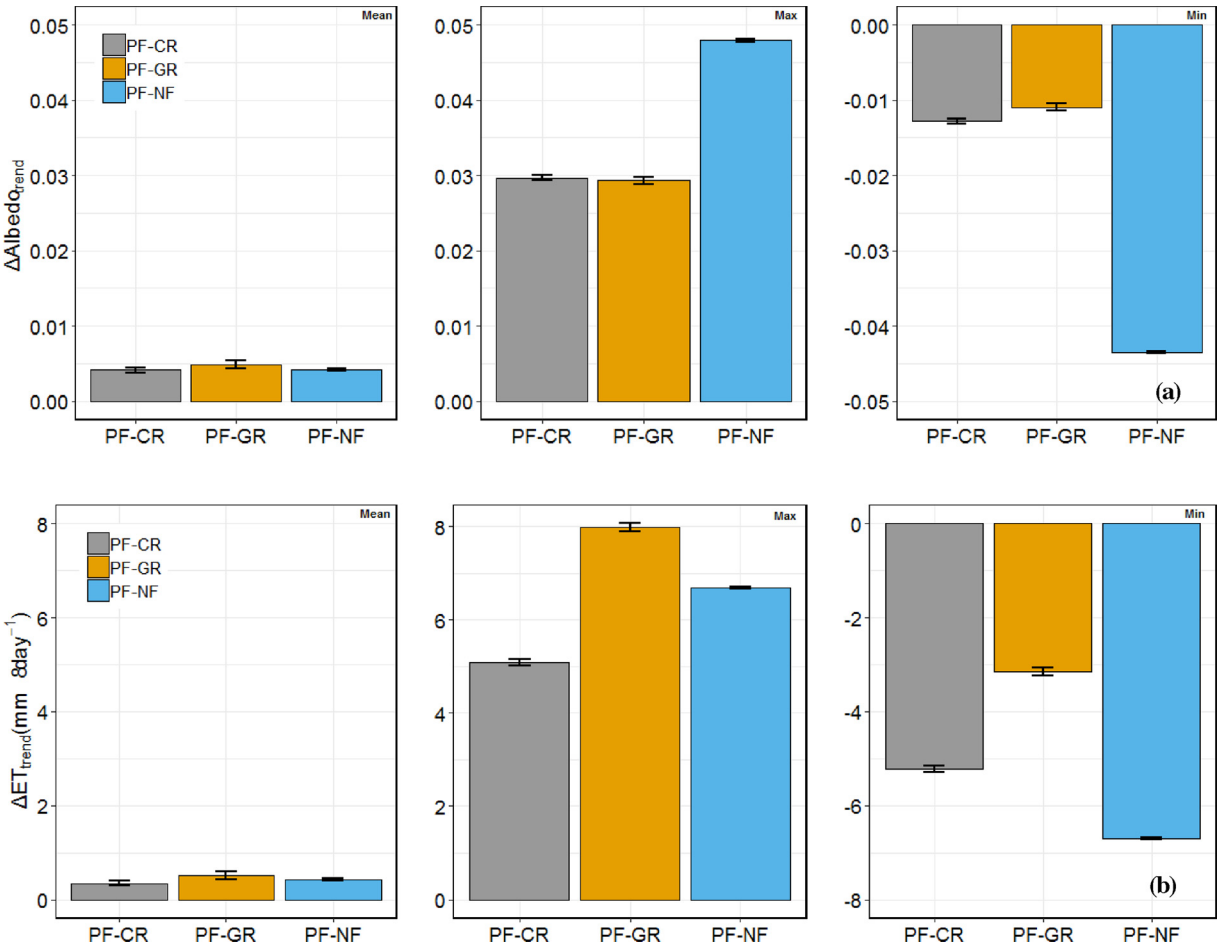

Fig. 9. Annual (mean, maximum, and minimum values) albedo differences ($\Delta Albedo_{trend}$, a) and ET differences (ΔET_{trend}, b) between plantation forests and the natural forests, cropland, and grassland in Guangdong Province, China, from 2000 to 2010. The vertical lines on each bar represent the confidence interval at 95% estimated by Student's *t* test.

investigate this situation, such as quantifying the actual change impacts of afforestation between afforested and nearby unchanged forest over several years on the LST change based on the window searching method (Li et al., 2016). However, Li et al. (2016) showed that the window searching method-based hypothetical change and actual change effects to forests had different impacts on maximum and minimum temperatures. Here, we used 2 temporal observations (2000–2010) to represent the actual change of PF on temperature at the pixel level.

4.2. Analysis of actual PF change in detecting temperature

Cooling effects in the spatial pattern varied from other forest and non-forest types to plantation forests from 2000 to 2010. Our results showing this was highly consistent with the existing research (Arora and Montenegro, 2011; Bonan, 2008). Specifically, daytime and nighttime cooling was found, especially for the LST difference of PF minus CR. It has been shown that replacing cropland with forests tends to produce cooler surface air temperatures (Lee et al., 2011; Wickham et al., 2012). However, a small warming effect between PF and GR during the daytime was detected in our study, which was controlled by the ET variations (Zhang and Liang, 2018). Although annual daytime warming was offset by nighttime cooling between PF and NF of about –0.01 °C ± 0.02 °C, a slight daytime warming (˜0.1 °C) and nighttime cooling (˜– 0.1 °C) was found. This daytime warming may be controlled by the specific temporal variation of afforestation from natural forests with different latitudes (Lee et al., 2011).

In the winter and autumn months (and especially in the winter), the strong warming effect explains the lack of a snow-albedo feedback (Peng et al., 2014). However, albedo showed a cooling effect (Fig. 10a) due to the ambiguous relationship of albedo in Fig.S9, while ET led to a warming effect (Fig. S9, Fig.10c). The temperature effect of albedo in the lower latitude warmer regions was almost negligible, especially in the tropical forests (Devaraju et al., 2015). The distinct cooling effect of increased ET during the spring and summer was produced (Perugini et al., 2017); for example, it was reported due to the replacement of cropland with forest in western Guangdong (Fig. 5a and b, Fig. 8a), except that an opposite warming effect was found in tropical forest in summer due to the drought on the Leizhou Peninsula of southern Guangdong Province (Zhang et al., 2017).

In the dry season, there was a warming effect due to afforestation changes, and during the wet season, we observed the opposite trend (Fig. S8). There was evidence that the trend was mostly affected by ET, including that there was a large leaf index and high transpiration rate during the wet season causing a greater cooling effect than the warming effect of albedo (Arora and Montenegro, 2011). Evergreen trees are a dominant species in Guangdong Province, but they are rarely covered by snow compared to deciduous trees. Consequently, the warming effect of albedo occurs (Tang et al., 2018; Zhao and Jackson, 2014). This inverse relationship can be balanced when open lands transition to plantation forests. Plantation forests with lower albedo absorb the majority of incoming solar energy, which is released as sensible heat and triggers a warming effect (Bonan, 2008). However, plantation forests also emit water vapor through ET, which acts to cool the surface (Perugini et al., 2017). For tropical forests (e.g., southern China), strong

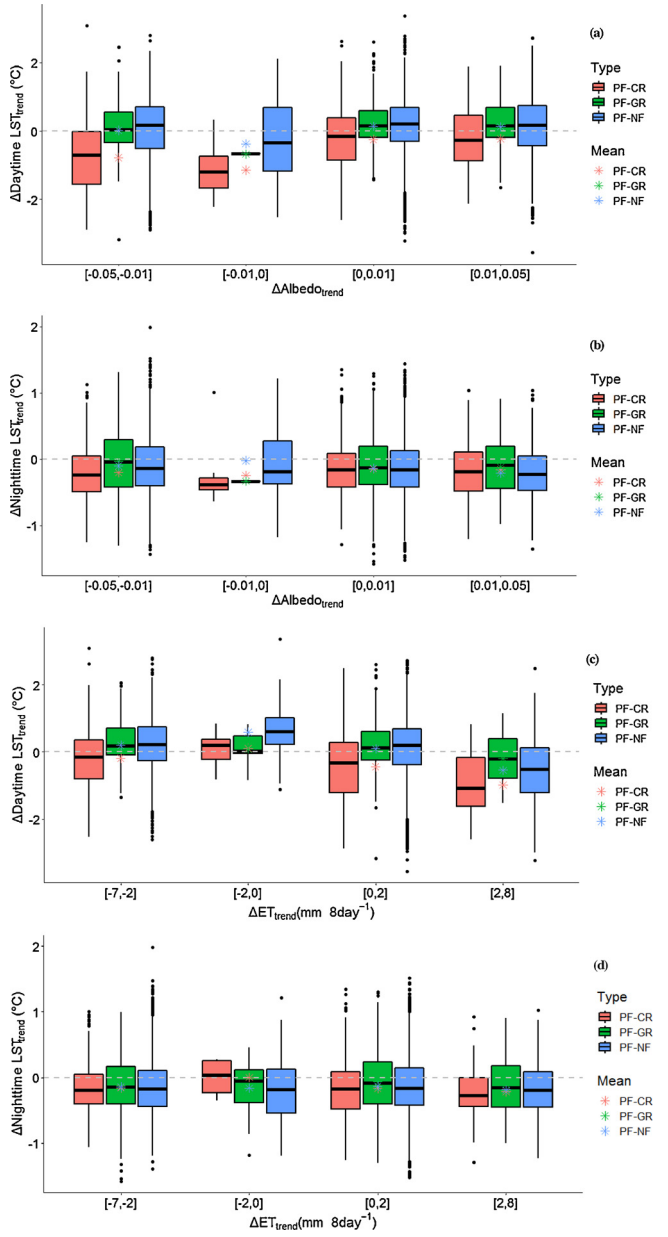

Fig. 10. Boxplot illustrating the relationship between annual ΔDaytime LST_{trend} and ΔNighttime LST_{trend}, and different annual $\Delta Albedo_{trend}$ (a, b) and ΔET_{trend} (c, d) ranges of the changes of plantation forests, natural forests, cropland, and grassland from 2000 to 2010, showing the mean (star), median (thick black line), and the lower and upper 25 percentiles (thin lines), and maximum and minimum values (black point).

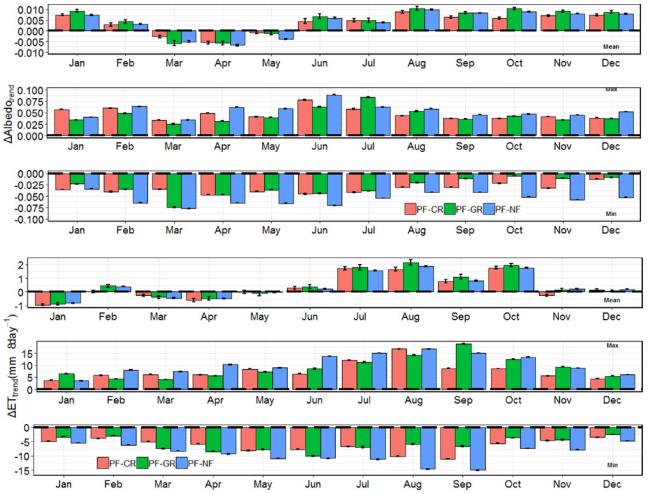

Fig. 11. Monthly albedo and ET differences between plantation forests, natural forests, cropland, and grassland in Guangdong Province, China, from 2000 to 2010. The vertical lines on each bar represent the confidence interval at 95% estimated by Student's *t* test.

evaporative cooling was the dominant cooling effect (Arora and Montenegro, 2011; Bala et al., 2007; Betts, 2006; Bonan, 2008; Davin and de Noblet-Ducoudré, 2010; Ma et al., 2017).

Reduced warming was observed due to afforestation in the mid-subtropical forest zone to tropical forest zone, a finding was consistent with other studies of surface temperature between 20 °N and 50 °N (Li et al., 2016). The warming effect from afforestation in the mid-subtropical forest zone illustrated that a transitional latitude (north of 24 °N) caused the warming effect to transfer to a cooling effect. The transitional latitude that separates cooling and warming moved southward, which differed from the findings of Li et al. (2015) (north of 45 °N) and Lee et al. (2011) (north of 55 °N). The area of natural forests in northern Guangdong showed a downward trend (2002–2012) in the mid-subtropical forest zone, according to the forestry statistical data of Guangdong Province, due to wood demand for an increasing population and the ecological reconstruction by removing most of the natural forests as plantation forests, the majority of which consist of fast-growing and high-yield tree species (CSF, 2014). These reasons explain the changed LST impacts between PF and NF in Fig. 5a. The increasing temperature between PF and NF was higher than that of CR and GR from 2000 to 2010. We assumed that the low albedo of afforested conifer forests with dark leaves (that absorb more sunlight than the underlying ground) led to the warming effect in northern Guangdong (Popkin, 2019). Due to the possible positive correlation between ΔET_{trend} and $\Delta Precipitation_{trend}$ (Fig. 13d), we showed that a strong ET cooling effect (Fig. S10) can be constrained under dry conditions. This suggests warming is more likely to occur in dry regions that are under moisture stress and experience shortwave radiation (Li et al., 2015; Peng et al., 2014). Fig. S11 also shows the warming effect of negative ΔET in spring, which can be explained by the fact that Nanling mountains in northern Guangdong block the formation of precipitation in the spring, causing spring drought from north to south (Gao et al., 2008). Otherwise, the karst topography and soil erosion in northern Guangdong does not store water and supplement precipitation, and young forests and plantations are likely to decrease water flow (Stolton and Dudley, 2007) and limit evaporation. Meanwhile, the decreasing area of cropland and the transition to plantation forests were detected, especially in a widely distributed area of cropland in western Guangdong near the border of the south-subtropical and tropical forest zone (Fig. 5a), due to tree planting accompanied by urbanization expansion into cropland (CSF, 2014), leading to a greater cooling effect than afforestation from grassland and natural forests. One reason for this is that forests have higher surface roughness due to taller canopies than croplands, thereby promoting greater heat dissipation (Lee et al., 2011). Another reason is the fact that forests with deep roots have higher transpiration rates than croplands, while grasslands mainly rely on shallow soil water due to their limited root system (Bonan, 2008). Therefore, afforestation in Guangdong from 2000 to 2010 led to net cooling, and warming in the dry regions was offset by wet regions cooling.

4.3. Driving effects of air temperature and precipitation on climate changes associated with PF

A limited number of air temperature and precipitation observations can be collected and usually do not coincide with the locations of plantation forest changes (Li et al., 2016). It was therefore difficult to

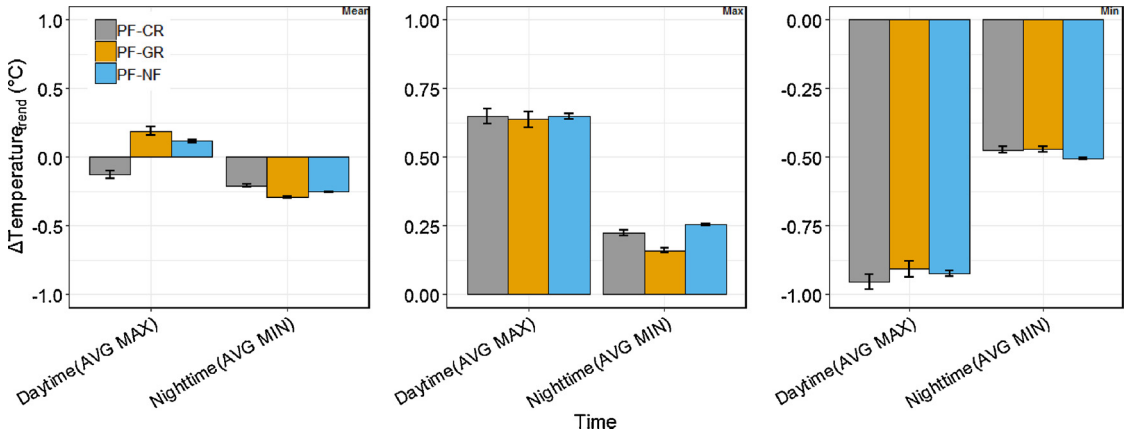

Fig. 12. Annual (mean, maximum, and minimum values) land surface temperature differences (ΔDaytime (AVG MAX) LST_{trend} and ΔNighttime (AVG MIN) LST_{trend}) between plantation forests and the natural forests, cropland, and grassland in Guangdong Province, China, from 2000 to 2010. The vertical lines on each bar represent the confidence interval at 95% estimated by Student's *t* test.

assess the impacts of plantation forest changes on *in situ* measurements. Usually either the Climate Research Unit (CRU) climate dataset or the Global Historical Climatology Network have been selected to explore the relationship between LST and *in situ* measurements (Li et al., 2016, 2015; Peng et al., 2014; Tang et al., 2018); For example, the CRU TS3.10 dataset has been interpolated based on station anomalies from 1961 to 1990 (Harris et al., 2014). Moreover, RF-based air temperature and precipitation interpolated maps for 2000 and 2010 were developed and fit with changes in afforestation. Both of LST and air temperature had a similar cooling effect on the increasing plantation forests (Mildrexler et al., 2011), but a smaller effect on air temperature was detected than that on LST (Lee et al., 2011; Perugini et al., 2017). This indicated the existence of complex and ambiguous relationships caused by the mismatching between the maximum and minimum temperature and time of overpass (Vancutsem et al., 2010), as illustrated in Fig. S12.

The warming effect observed in relatively dry regions was examined (Fig. 7), but we also detected a major cooling effect, which we attributed to the positive relationship between ET and precipitation in wet regions. This illustrates the vital role of the background climate, such as precipitation (Perugini et al., 2017). Strong precipitation results in moist soils for vegetation growth, which leads to high rates of latent fluxes and triggers a cooling surface (Forzieri et al., 2017). The relationship of the decreasing LST and decreasing precipitation was found in Fig. 13a and b, showing that there were other factors modulating climate patterns and processes, such as snow or cloud cover (Zhang and Liang, 2018; Zhou et al., 2012).

4.4. Uncertainties and future works

A real and effective forest cover map is the basic requirement of this study. Elevation differences on the temperature were not discussed, even if limited effect has been shown (Peng et al., 2014). Further, combing 2 types of temperature data—meteorological station-based interpolated temperature and satellite observation-based land surface temperature—would deduce the robust temperature map (Vancutsem et al., 2010). The decrease in temperature due to afforestation has been noted in the short term (10 years of temporal record and average for 16-year temporal domain) in southern China. Our results are not consistent with most climate models (Bonan, 1997; Yin et al., 2018). For instance, Yin et al. (2018) indicated that climate change risk to forests was concentrated in southern China based on the scenario-based climate model (e.g., RCP8.5) as the degree of warming increased in the 21th century, due to the intensified dryness. The biophysical effect of the changes in forest cover (afforestation, reforestation, or deforestation) on temperature needs to be balanced, and should account for the mitigation effects of climate extremes being comparable to terrestrial carbon sinks (Alkama and Cescatti, 2016). Hence, the combination of satellite observations, such as sensible and latent heat, surface roughness, and albedo, climate model, detailed background climate, and *in situ* measurements, such as flux towers, station observations, as well as tree species and tree densities could reveal much about abundant plantation forest-climate interactions (Alkama and Cescatti, 2016; Burakowski et al., 2018).

5. Conclusions

In this work, we proposed two methods to quantify plantation forest changes and their impact on surface temperature change in Guangdong Province, southern China. Namely, we used the moving window method at the sample grid cell level, as well as the temporal-spatial pattern change analysis method at the pixel level, to determine the hypothetical change effect and actual change effect, respectively. Using these methods for the changes caused by afforestation, the overall consistency of the cooling effect was evaluated. The latter method supported the characterization of the actual change pattern of plantation forests and generated the detailed and robust diurnal and seasonal discrepancies of afforestation on surface temperature, especially a cooling effect by afforestation from croplands. Meanwhile, the decreasing temperatures varied with latitudinal direction, in spite of the warming effect in mid-subtropical forests. Dry season warming of albedo was balanced by the wet season cooling of ET, and ET dominated the cooling effect in the warm season and in the tropical forests. An inequable cooling effect was detected between air temperature and surface temperature. Precipitation appeared to play a crucial part in ET-triggered temperature decrease in the humid southern China region. Although combining the satellite observations and *in situ* measurements to detect the effects of afforestation on temperature has some challenges, exploring the biophysical effects of forest cover changes from afforestation on temperature guide forest management and protection for policy makers. This is especially the case for those located in plantation forest regions in southern China and other plantation forest regions. It is beneficial to understand and exert potential trade-offs or synergies of climate adaptation and mitigation in subtropical and tropical regions and at a global level.

Acknowledgements

Our work was jointly funded or supported by the National Natural Science Foundation of China (31670552, 41771379), the China Postdoctoral Science Foundation funded project, and the PAPD (Priority Academic Program Development) of Jiangsu provincial universities. Special thanks need to go to the Land Processes Distributed

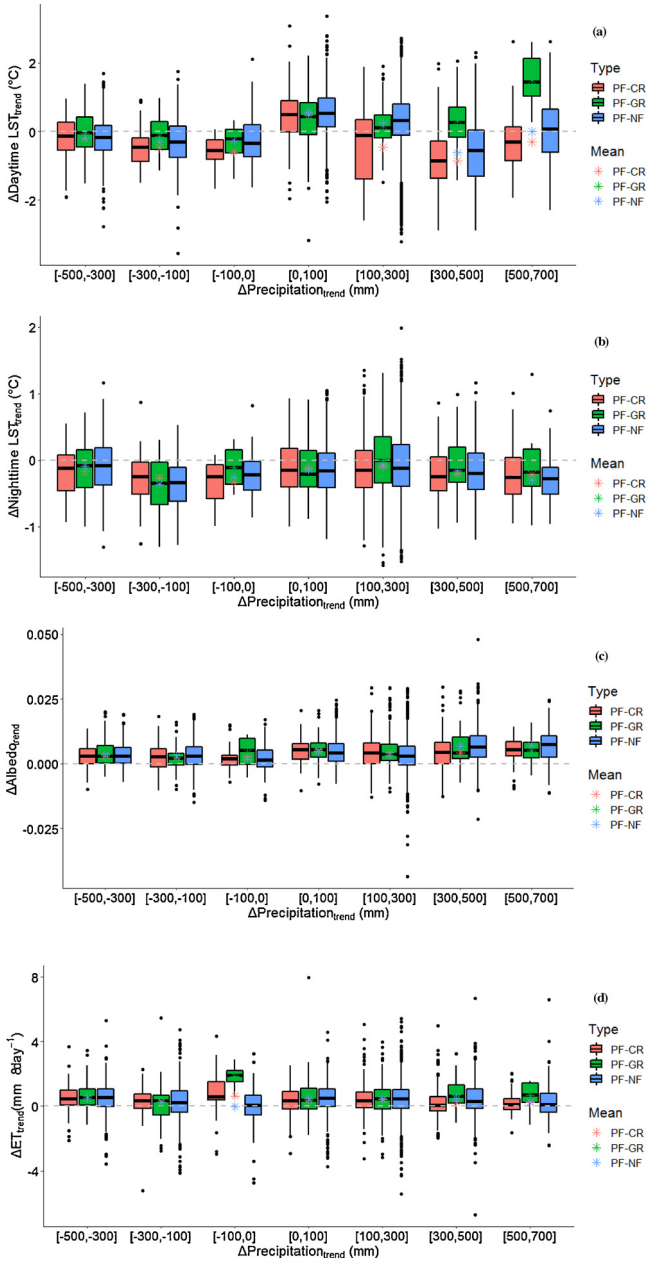

Fig. 13. Boxplot for annual Δdaytime LST$_{trend}$ (a), Δnighttime LST$_{trend}$ (b), ΔAlbedo$_{trend}$ (c), and ΔET$_{trend}$ (d) during 2000–2010 between plantation forests, natural forests, cropland, and grassland for different annual ΔPrecipitation$_{trend}$ ranges showing the mean (star), median (thick black line), and the lower and upper 25 percentiles (thin lines), and maximum and minimum values (black point).

Active Archive Center, they provided the MODIS data. The authors also thank the Guangdong Provincial Center for Forest Resources Monitoring for providing field inventories and Dr. Yan Li in Beijing Normal University, China in provision of the aid of methods interpretation and paper editing. Additionally, this work was performed while the corresponding author acted as an awardee of the 2017 Qinglan project sponsored by Jiangsu Province.

Appendix A. Supplementary data

Supplementary material related to this article can be found, in the online version, at doi:https://doi.org/10.1016/j.agrformet.2019.107641.

References

Alkama, R., Cescatti, A., 2016. Biophysical climate impacts of recent changes in global forest cover. Science 351, 600–604.
Arora, V.K., Montenegro, A., 2011. Small temperature benefits provided by realistic afforestation efforts. Nat. Geosci. 4, 514–518.
Bala, G., Caldeira, K., Wickett, M., Phillips, T.J., Lobell, D.B., Delire, C., Mirin, A., 2007. Combined climate and carbon-cycle effects of large-scale deforestation. PNAS 104, 6550–6555.
Banskota, A., Kayastha, N., Falkowski, M.J., Wulder, M.A., Froese, R.E., White, J.C., 2014. Forest monitoring using Landsat time series Data: a review. Can. J. Remote Sens. 40, 362–384.
Betts, R.A., 2001. Biogeophysical impacts of land use on present-day climate: near-surface temperature change and radiative forcing. Atmos. Sci. Lett. 2, 39–51.
Betts, R.A., 2006. Forcings and feedbacks by land ecosystem changes on climate change. J. Phys. IV (Proceedings) 139, 119–142.
Bonan, G.B., 1997. Effects of land use on the climate of the United States. Clim. Change 37, 449–486.
Bonan, G.B., 2008. Forests and climate change forcings, feedbacks, and the climate benefits of forests. Science 320, 1444–1449.
Brown, S., Lugo, A.E., Chapman, J.D., 1986. Biomass of tropical tree plantation and its implications for the global carbon budget. Can. J. For. Res. 16, 390–394.
Burakowski, E., Tawfik, A., Ouimette, A., Lepine, L., Novick, K., Ollinger, S., Zarzycki, C., Bonan, G., 2018. The role of surface roughness, albedo, and Bowen ratio on ecosystem energy balance in the Eastern United States. Agric. For. Meteorol. 249, 367–376.
Chen, J., Chen, J., Liao, A., Cao, X., Chen, L., Chen, X., He, C., Han, G., Peng, S., Lu, M., Zhang, W., Tong, X., Mills, J., 2015. Global land cover mapping at 30m resolution: a POK-based operational approach. ISPRS J. Photogramm. 103, 7–27.
Coppin, P., Jonckheere, I., Nackaerts, K., Muys, B., Lambin, E., 2004. Digital change detection methods in ecosystem monitoring: a review. Int. J. Remote Sens. 25, 1565–1596.
CSF, 2014. China Forest Resources Report: the 8th National Inventory of Forest Resources. China Forestry Publishing House, Beijing.
Davin, E.L., de Noblet-Ducoudré, N., 2010. Climatic impact of global-scale deforestation: radiative versus nonradiative processes. J. Clim. 23, 97–112.
Deng, Y., Wang, S., Bai, X., Tian, Y., Wu, L., Xiao, J., Chen, F., Qian, Q., 2018. Relationship among land surface temperature and LUCC, NDVI in typical karst area. Sci. Rep.-Uk 8, 641.
Devaraju, N., Bala, G., Nemani, R., 2015. Modelling the influence of land-use changes on biophysical and biochemical interactions at regional and global scales. Plant Cell Environ. 38, 1931–1946.
Duveiller, G., Hooker, J., Cescatti, A., 2018. The mark of vegetation change on Earth's surface energy balance. Nat. Commun. 9, 679.
Forzieri, G., Alkama, R., Miralles, D.G., Cescatti, A., 2017. Satellites reveal contrasting responses of regional climate to the widespread greening of Earth. Science 356, 1180–1184.
Gao, M., Qin, Z., Zhang, H., Lu, L., Zhou, X., Yang, X., 2008. Remote sensing of agro-droughts in Guangdong Province of China using MODIS satellite data. Sensors (Basel) 8, 4687–4708.
Geng, L., Ma, M., Yu, W., Wang, X., Jia, S., 2014. Validation of the MODIS NDVI products in different land-use types using in situ measurements in the Heihe River Basin. IEEE Geosci. Remote Sens. Lett. 11, 1649–1653.
Hansen, M.C., Potapov, P.V., Moore, R., Hancher, M., Turubanova, S.A., Tyukavina, A., Thau, D., Stehman, S.V., Goetz, S.J., Loveland, T.R., Kommareddy, A., Egorov, A., Chini, L., Justice, C.O., Townshend, J.R., 2013. High-resolution global maps of 21st-century forest cover change. Science 342, 850–853.
Harris, I., Jones, P.D., Osborn, T.J., Lister, D.H., 2014. Updated high-resolution grids of monthly climatic observations - the CRU TS3.10 Dataset. Int. J. Climatol. 34, 623–642.
Homer, C., Dewitz, J., Fry, J., Coan, M., Hossain, N., Larson, C., et al., 2007. Completion of the 2001 national land cover database for the Conterminous United States. Photogramm. Eng. Remote Sens. 73, 337.
Jackson, R.B., Randerson, J.T., Canadell, J.G., Anderson, R.G., Avissar, R., Baldocchi, D.D., Bonan, G.B., Caldeira, K., Diffenbaugh, N.S., Field, C.B., Hungate, B.A., Jobbágy, E.G., Kueppers, L.M., Nosetto, M.D., Pataki, D.E., 2008. Protecting climate with forests. Environ. Res. Lett. 3, 044006.
Justice, C.O., Vermote, E., Townshend, J.R., Defries, R., Roy, D.P., Hall, D.K., et al., 1998. The Moderate Resolution Imaging Spectroradiometer (MODIS): Land remote sensing for global change research. IEEE Trans. Geosci. Remote Sens. 36, 1228–1249.
Lee, X., Goulden, M.L., Hollinger, D.Y., Barr, A., Black, T.A., Bohrer, G., Bracho, R., Drake, B., Goldstein, A., Gu, L., Katul, G., Kolb, T., Law, B.E., Margolis, H., Meyers, T., Monson, R., Munger, W., Oren, R., Paw, U.K., Richardson, A.D., Schmid, H.P., Staebler, R., Wofsy, S., Zhao, L., 2011. Observed increase in local cooling effect of deforestation at higher latitudes. Nature 479, 384–387.
Li, Y., Zhao, M., Mildrexler, D.J., Motesharrei, S., Mu, Q., Kalnay, E., Zhao, F., Li, S., Wang, K., 2016. Potential and actual impacts of deforestation and afforestation on land surface temperature. J. Geophys. Res. Atmos. 121 (14), 386 372-314.
Li, Y., Zhao, M., Motesharrei, S., Mu, Q., Kalnay, E., Li, S., 2015. Local cooling and warming effects of forests based on satellite observations. Nat. Commun. 6, 6603.
Li, Z., Tang, B., Wu, H., Ren, H., Yan, G., Wan, Z., Trigo, I.F., Sobrino, J.A., 2013. Satellite-derived land surface temperature: current status and perspectives. Remote Sens. Environ. 131, 14–37.
Liu, J., Schaaf, C., Strahler, A., Jiao, Z., Shuai, Y., Zhang, Q., Roman, M., Augustine, J.A., Dutton, E.G., 2009. Validation of Moderate Resolution Imaging Spectroradiometer

(MODIS) albedo retrieval algorithm: dependence of albedo on solar zenith angle. J. Geophys. Res. Atmos. 114.
Liu, Z., Ballantyne, A.P., Cooper, L.A., 2019. Biophysical feedback of global forest fires on surface temperature. Nat. Commun. 10, 214.
Ma, W., Jia, G., Zhang, A., 2017. Multiple satellite-based analysis reveals complex climate effects of temperate forests and related energy budget. J. Geophys. Res. Atmos. 122, 3806–3820.
Mildrexler, D.J., Zhao, M., Running, S.W., 2011. A global comparison between station air temperatures and MODIS land surface temperatures reveals the cooling role of forests. J. Geophys. Res. 116.
Mu, Q.Z., Zhao, M.S., Running, S.W., 2011. Improvements to a MODIS global terrestrial evapotranspiration algorithm. Remote Sens. Environ. 115, 1781–1800.
Ndossi, M., Avdan, U., 2016. Inversion of land surface temperature (LST) using terra ASTER data: a comparison of three algorithms. Remote Sens. 8, 993.
Pal, S., Ziaul, S., 2017. Detection of land use and land cover change and land surface temperature in English Bazar urban centre. Egypt. J. Remote. Sens. Space Sci. 20, 125–145.
Peng, S.S., Piao, S., Zeng, Z., Ciais, P., Zhou, L., Li, L.Z., Myneni, R.B., Yin, Y., Zeng, H., 2014. Afforestation in China cools local land surface temperature. PNAS 111, 2915–2919.
Perugini, L., Caporaso, L., Marconi, S., Cescatti, A., Quesada, B., de Noblet-Ducoudré, N., House, J.I., Arneth, A., 2017. Biophysical effects on temperature and precipitation due to land cover change. Environ. Res. Lett. 12, 053002.
Piao, S.L., Fang, J.Y., Ciais, P., Peylin, P., Huang, Y., Sitch, S., Wang, T., 2009. The carbon balance of terrestrial ecosystems in China. Nature 458, 1009–1013.
Popkin, G., 2019. How much can forest fight climate change? Trees are supposed to slow global warming, but growing evidence suggests they might not always be climate saviours. Nature 565, 280–282.
Schaaf, C.B., Gao, F., Strahler, A.H., Lucht, W., Li, X., Tsang, T., Lewis, P., 2002. First operational BRDF, albedo nadir reflectance products from MODIS. Remote Sens. Environ. 83, 135–148.
Shen, W., Li, M., Huang, C., Tao, X., Li, S., Wei, A., 2019. Mapping annual forest change due to afforestation in Guangdong Province of China using active and passive remote sensing data. Remote Sens. 11, 490.
Shen, W., Li, M., Huang, C., Tao, X., Wei, A., 2018. Annual forest aboveground biomass changes mapped using ICESat/GLAS measurements, historical inventory data, and time-series optical and radar imagery for Guangdong province, China. Agric. For. Meteorol. 259, 23–38.
Sobrino, J.A., Jiménez-Muñoz, J.C., Paolini, L., 2004. Land surface temperature retrieval from Landsat TM 5. Remote Sens. Environ. 90, 434–440.
Song, Z., Li, R., Qiu, R., Liu, S., Tan, C., Li, Q., Ge, W., Han, X., Tang, X., Shi, W., Song, L., Yu, W., Yang, H., Ma, M., 2018. Global land surface temperature influenced by vegetation cover and PM2.5 from 2001 to 2016. Remote Sens. 10, 2034.
Stolton, S., Dudley, N., 2007. Managing forests for cleaner water for urban populations. Unasylva 58, 39–43.
Swann, A.L., Fung, I.Y., Chiang, J.C., 2012. Mid-latitude afforestation shifts general circulation and tropical precipitation. PNAS 109, 712–716.
Tang, B., Zhao, X., Zhao, W., 2018. Local effects of forests on temperatures across Europe. Remote Sens. 10, 529.
Tomlinson, C.J., Chapman, L., Thornes, J.E., Baker, C., 2011. Remote sensing land surface temperature for meteorology and climatology: a review. Meteorol. Appl. 18, 296–306.
van Leeuwen, T.T., Frank, A.J., Jin, Y., Smyth, P., Goulden, M.L., van der Werf, G.R., Randerson, J.T., 2011. Optimal use of land surface temperature data to detect changes in tropical forest cover. J. Geophys. Res. Biogeosci. 116.
Vancutsem, C., Ceccato, P., Dinku, T., Connor, S.J., 2010. Evaluation of MODIS land surface temperature data to estimate air temperature in different ecosystems over Africa. Remote Sens. Environ. 114, 449–465.
Wan, Z., 2008. New refinements and validation of the MODIS land-surface temperature/emissivity products. Remote Sens. Environ. 112, 59–74.
Wickham, J.D., Wade, T.G., Riitters, K.H., 2012. Comparison of cropland and forest surface temperatures across the conterminous United States. Agric. For. Meteorol. 166, 137–143.
Wickham, J.D., Wade, T.G., Riitters, K.H., 2013. Empirical analysis of the influence of forest extent on annual and seasonal surface temperatures for the continental United States. Global Ecol. Biogeogr. 22, 620–629.
Yin, Y., Ma, D., Wu, S., 2018. Climate change risk to forests in China associated with warming. Sci. Rep.-Uk 8, 493.
Zeng, W., Tomppo, E., Healey, S.P., Gadow, K.V., 2015. The national forest inventory in China: history - results - international context. For. Ecosyst. 2, 23.
Zhang, H., Cheng, W., Qiu, X., Feng, X., Gong, W., 2017. Tide-surge interaction along the east coast of the Leizhou Peninsula, South China Sea. Cont. Shelf Res. 142, 32–49.
Zhang, Y., Liang, S., 2018. Impacts of land cover transitions on surface temperature in China based on satellite observations. Environ. Res. Lett. 13, 024010.
Zhao, K., Jackson, R., 2014. Biophysical forcings of land-use changes from potential forestry activities in North America. Ecol. Monogr. 84, 329–353.
Zhou, L., Tian, Y., Baidya Roy, S., Thorncroft, C., Bosart, L.F., Hu, Y., 2012. Impacts of wind farms on land surface temperature. Nat. Clim. Change 2, 539–543.